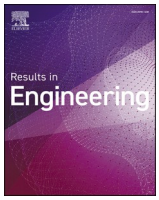
Results in Engineering 23 (2024) 102639



Contents lists available at ScienceDirect

Results in Engineering

journal homepage: www.sciencedirect.com/journal/results-in-engineering





CFD study of the effect of leading-edge tubercles on the aerodynamic characteristics of a small UAV based on eppler 186 airfoils

Rafael Bardera [a], Ángel Antonio Rodríguez-Sevillano [b], Estela Barroso-Barderas [a], Juan Carlos Matías-García [a,*]

[a] Instituto Nacional de Técnica Aeroespacial, Torrejón de Ardoz, Spain
[b] Escuela Técnica Superior de Ingeniería Aeronáutica y del Espacio. Universidad Politécnica de Madrid (UPM), Madrid, Spain

ARTICLE INFO

Keywords:
Tubercles
Biomimetic
CFD

ABSTRACT

A numerical analysis is carried out to evaluate the aerodynamic characteristics of a small Unmanned Aerial Vehicle (UAV) whose wings are modified to incorporate sinusoidal leading edges (tubercles). This UAV has a rectangular wing composed of Eppler 186 airfoils. The aerodynamic characteristics of four UAV configurations varying the wavelength and amplitude along the wingspan are evaluated using Computational Fluid Dynamics (CFD). Results are compared with the baseline case, that is, without leading-edge tubercles. The wing configurations with tubercles exhibited increased lift at high angles of attack and delayed stall. The configuration with maximum amplitude ($a = 0.05c$) and minium wavelength ($\lambda = 0.25c$) achieved an increase up to 17 % in the maximum lift coefficient and delayed the stall up to the angle of attack of 20° compared to the baseline case.

1. Introduction

Unmanned Aerial Vehicles (UAVs) have evolved significantly, transitioning from their initial military applications to widespread use in commercial activities, driven by technological progress. They play crucial roles in executing tasks in hazardous or challenging environments, reducing human risks [1,2]. However, the aerodynamics of small UAVs present challenges due to their size and operational velocities, characterized by low Reynolds numbers (Re) [3]. This requires innovative design solutions to effectively balance these factors. Consequently, bioinspired UAV designs that mimic nature are rapidly evolving [4].

Inspired by nature, particularly the ventral fins of humpback whales featuring tubercled leading-edges, researchers have explored incorporating similar tubercle designs into UAV lifting bodies [5]. These tubercles are believed to enhance lift during prey-catching maneuvers, enabling sharp turns without losing lift. Various studies have demonstrated aerodynamic benefits, particularly in improving stall characteristics. Research on leading-edge modifications with tubercles has been ongoing for the past decade, driven by their potential for flow control. Extensive literature exists, encompassing experimental and numerical simulation studies aimed at quantifying performance enhancement and understanding the flow-control mechanism of these tubercles.

Moscato et al. [6] tested modified wing/blade geometries with leading-edge artificial bumps to address the observed reduction in lift coefficient before stall compared to standard wings. Several tubercle geometries were tested, evaluating overall forces on the wings, which indicated performance improvements for all trailing edge tubercle geometries. Similarly, Miklosovic et al. [7] conducted experiments demonstrating that adding tubercles to a humpback whale flipper model delayed stall angles by 40 %, increased lift, and reduced drag. Idealized scale models of the flipper with and without tubercles in a specific Re range were used.

Wei and et al. [8] examined experimentally the impact of leading-edge tubercles on aerodynamic performance and surface flow structures of tapered swept-back wings across various Re numbers. They observed minimal variation in lift and drag curve behaviour for the baseline wing when $Re > 8.2 \bullet 10^4$. However, wings with tubercles slightly improved aerodynamic performance within a lower angle of attack range $(2° < \alpha < 7°)$ and enhanced stall behavior at $\alpha < 20°$. Surface flow patterns revealed complex vortex structures and critical points at moderate angles of attack, influenced by the leading-edge tubercle orientation and sweep-angle. Additionally, Seyhan et al. [9] conducted an experimental investigation into the effects of leading-edge

* Corresponding Author.
E-mail addresses: barderar@inta.es (R. Bardera), angel.rodriguez.sevillano@upm.es (Á.A. Rodríguez-Sevillano), barrosobe@inta.es (E. Barroso-Barderas), matiasgjc@inta.es (J.C. Matías-García).

https://doi.org/10.1016/j.rineng.2024.102639
Received 16 June 2024; Received in revised form 25 July 2024; Accepted 27 July 2024
Available online 2 August 2024
2590-1230/© 2024 The Authors. Published by Elsevier B.V. This is an open access article under the CC BY-NC-ND license (http://creativecommons.org/licenses/by-nc-nd/4.0/).

Nomenclature

CFD	: Computational Fluid Dynamics
INTA	: Instituto Nacional de Técnica Aeroespacial
UAV	: Unmanned Aerial Vehicle
UPM	: Universidad Politécnica de Madrid
a	: Maximum amplitude of tubercles
b	: Wingspan
c	: Chord
l	: Total length of the UAV
C_L	: Lift Coefficient
C_D	: Drag Coefficient
E	: Aerodynamic Efficiency
F	: Sinusoidal function of tubercles
S	: Wing surface
U_∞	: Free stream velocity
α	: Angle of attack
λ	: Minimum amplitude of tubercles
ρ	: Air density

tubercles on a tapered swept-back SD7032 airfoil at low Reynolds numbers. They found that airfoil models featuring leading-edge tubercles notably enhanced lift curves across various angles of attack in comparison to the baseline case. The presence of tubercles caused streamwise vortices, thereby increased turbulence and improved momentum exchange within the boundary layer. Moreover, Murray et al. [10] conducted experimental work revealing that tubercles improved performance across various sweep angles, with a maximum lift increase of 9 % and 4 % for specific angles.

Sudhakar and Karthikeyan [11] explored the influence of tubercles on the flow field over a NACA-4415 airfoil. Their study at a $\mathrm{Re} = 1.2 \bullet 10^5$ indicated enhanced pressure recovery with the modified leading edge compared to the baseline configuration. In another study by the same authors [12], the aerodynamic performance of a typical UAV with modified wings featuring tubercles on the leading edge was analyzed. The wings with tubercles demonstrated increased lift, stall angle, and reduced drag compared to the baseline at $Re = 8 \bullet 10^5$, improving aerodynamic efficiency ($\frac{C_L}{C_D}$) by up to 25 %. Furthermore, Johari et al. [13] investigated tubercle wavelength and amplitude effects on flow separation for a modified airfoil, finding substantial increases in lift without added drag for angles exceeding the baseline stall angle.

Liu and et al. [14] explored the effects of wavy leading-edge protuberances on a Clark-y three-dimensional hydrofoil. The results demonstrated how protuberances, functioning as vortex generators, enhanced boundary-layer vorticity, thereby improving hydrofoil hydrodynamics. Meanwhile, Ni et al. [15] proposed an empirical model for predicting the lift coefficients of twisted airfoils with leading-edge tubercles, effectively validated through experimental data and corresponding CFD studies, aligning closely with verified results.

The objective of this work is to study the effect of a sinusoidal leading edge on a small UAV with a rectangular wing composed of Eppler 186 airfoils. The aerodynamic characteristics of various modified wing configurations are obtained by Computational Fluid Dynamics (CFD) simulations under different angles of attack at $\mathrm{Re} = 1.3 \bullet 10^5$. The key novelty lies on the comparative evaluation against a baseline UAV configuration without leading-edge tubercles. Remarkably, the configurations with tubercles demonstrated a significant enhancement in aerodynamic performance, particularly at high angles of attack.

This research pioneers the application of sinusoidal leading edges on UAV wings, providing valuable insights into their potential to improve lift and delay stall, thus contributing to the advancement of UAV aerodynamic design.

2. 2small UAV model

A small UAV with a rectangular wing composed of Eppler 186 airfoils and a V-tail is developed between the National Institute for Aerospace Technology (INTA) and the Technical University of Madrid (UPM) [16]. The configuration of this small UAV and its dimensions are presented in Fig. 1. The model presents a total length of $l = 275$ mm, wingspan of $b = 540$ mm and a wing chord of $c = 90$ mm.

The rectangular wing is modified to incorporate tubercles on the leading edge to simulate the ventral fins of humpback whales. The leading edge is modelled by using the sinusoidal function depending on the amplitude (a) and wavelength (λ) given in Eq. (1):

$$F = a \bullet \cos\left(\frac{2\pi x}{\lambda}\right) \tag{1}$$

In this study, the leading edge of the wing is modified with four different tubercle configurations. All of them present constant wavelength (λ) and amplitude (a) along the wingspan. The first configuration (A-UAV) has leading edge tubercles with amplitude $a = 0.03c$ and wavelength $\lambda = 0.5c$, the second (B-UAV) has amplitude $a = 0.03c$ and wavelength $\lambda = 0.25c$, the third (C-UAV) has amplitude $a = 0.05c$ and wavelength $\lambda = 0.5c$ and the last configuration (D-UAV) has amplitude $a = 0.05c$ and wavelength $\lambda = 0.25c$(see Fig. 2).

3. CFD study

The aerodynamic characteristics of the small UAV are obtained using ANSYS-Fluent software. Due to the freestream velocity (U_∞) consistently aligning with the chordwise direction and there is no propeller on the vehicle, only half of the model is computed, divided by a symmetry condition (Fig. 3), thus reducing memory, storage and processing requirements. All boundaries are placed far from the UAV model to prevent flow blockage and minimize negative boundary effects on the numerical solution. Consequently, the inlet boundary extends to a distance of 5c ahead of the vehicle, while the outlet boundary is 20c behind it. The side, top and bottom boundaries are modelled as walls. The dimensions of the computational domain and the boundary surfaces are presented in Fig. 3.

The spatial discretization of the computational domain demands an appropriate growth rate of cells. Specifically, the region near the surface of the vehicle must be refined with smaller cell sizes to accurately capture the velocity variations near the boundary layer. An unstructured mesh with tetrahedral cells is used in all computational domain. A maximum element size of 13 mm is imposed for the surfaces farthest from the model, while a sizing restriction of 1.2 mm is required near the surface model (Fig. 3). The unstructured mesh has approximately 5 million of elements in each simulation.

The simulations are computed with an inlet velocity of $U_\infty = 20$ m/s, resulting in a Reynolds number of $\mathrm{Re} = 1.3 \bullet 10^5$, characteristic of the normal operating regime for these types of vehicles. For boundary layer simulation, standard wall functions are applied, while calculations employ a two-equation turbulence model ($k - \omega$) with a combination of *Shear Stress Transport (SST)* equations.

The angle of attack is modified from $\alpha = -5^\circ$ to $\alpha = +30^\circ$ with a step of 5° by rotating the model with respect to the incident free stream velocity (U_∞) using the same computational domain. With each tubercle wing configuration, 8 angle of attack conditions are studied. Consequently, a total of 32 simulations are conducted taking a computation time approximately of 5 h in each case.

4. Results and discussion

4.1. Aerodynamic characteristics

Figs. 4–6 illustrate how wing leading edge tubercles affect the

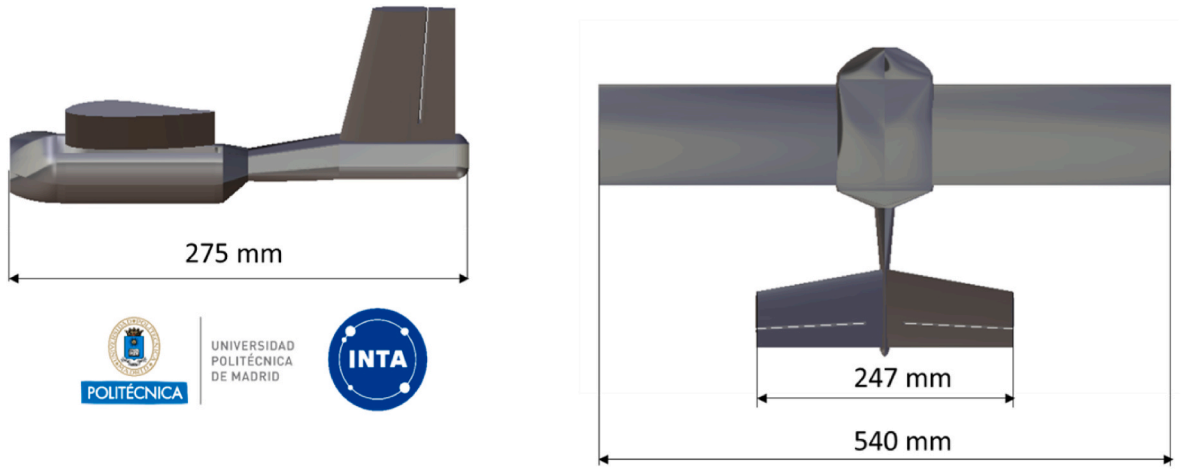


Fig. 1. Fixed-wing UAV designed by INTA and UPM.



Fig. 2. UAV configurations analyzed.

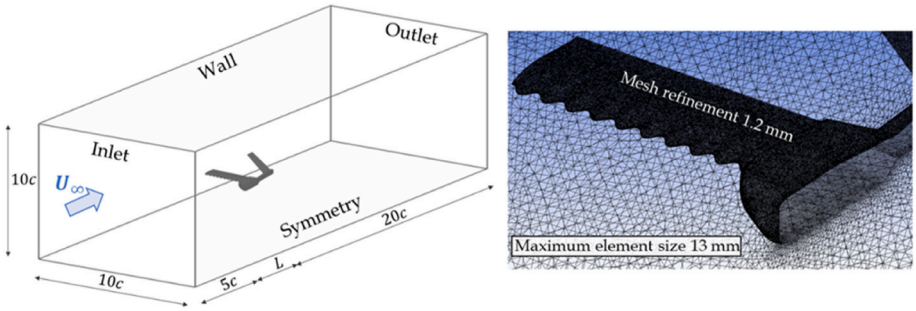


Fig. 3. Computational domain (left) and details of the unstructured mesh (right).

aerodynamic characteristics: lift, drag and aerodynamic efficiency (lift-to-drag ratio) of the UAV under study at Reynolds number $1.3 \bullet 10^5$.

The lift coefficient (C_L) for the four modified wing configurations and the baseline case is presented in Fig. 4. The coefficient curves indicate that the baseline wing (red curve) stalls at an angle of attack of about 10°, achieving a maximum lift coefficient of 0.79. All wing configurations show a linear increase in the lift coefficient with positive angles of attack up to $\alpha = 10°$. Below this angle of attack ($\alpha < 10°$), the baseline

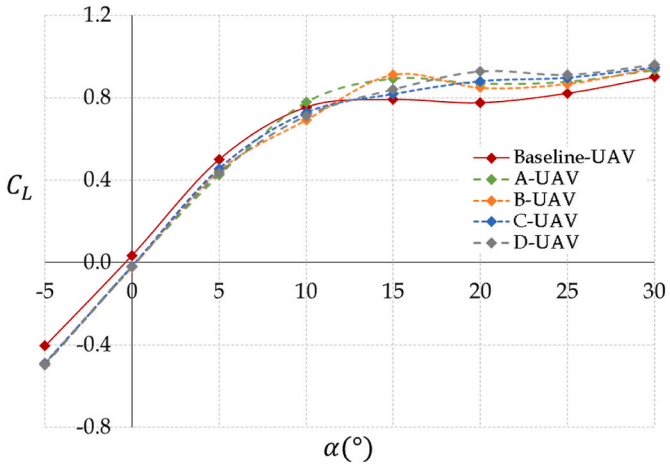


Fig. 4. Lift coefficient for baseline and four sinusoidal leading-edge configurations.

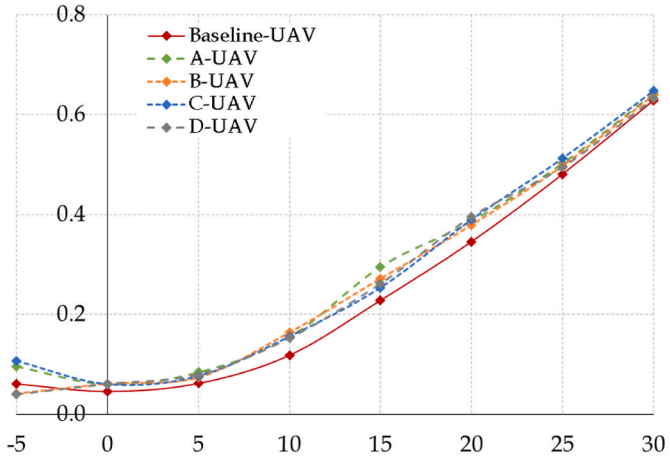


Fig. 5. Aerodynamic drag coefficient for baseline and four sinusoidal leading-edge configurations.

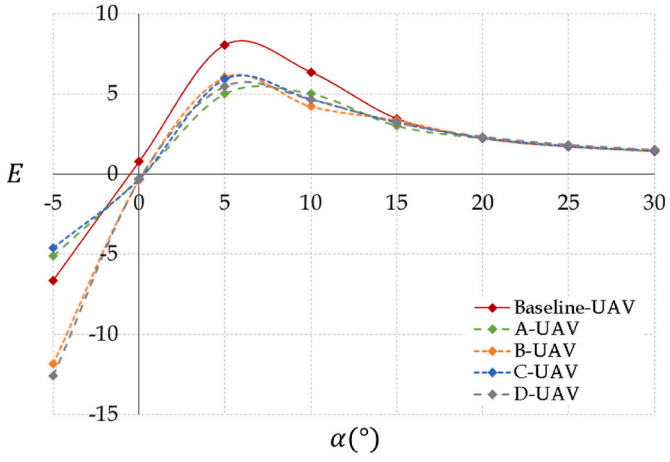


Fig. 6. Aerodynamic efficiency for baseline and four sinusoidal leading-edge configurations.

case shows higher values in the lift coefficient compared to the wing configurations with tubercles (A, B, C and D-UAV). This difference may be attributed to a change in the effective shape (increase in camber) of the airfoil section due to the laminar separation bubble on the upper surface of the baseline wing. In contrast, the presence of tubercles on the modified wing configurations reduces the extent and size of this separation bubble.

When the baseline wing stalls at $\alpha = 10°$, the lift coefficient is slightly higher than for all wings with tubercles except to the A-UAV configuration (green curve), in which the lift coefficient is approximately 2.5 % higher than the baseline wing.

In the post-stall region ($\alpha > 10°$), the modified wings demonstrate superior lift characteristics compared to the baseline case. The modified wing UAV configurations exhibit a delay in stall and an increase in the lift coefficient. The A and B UAV configurations (both with amplitude, $a = 0.03c$) delay stall entry up to $\alpha = 15°$ with reference to the baseline wing ($\alpha = 10°$) with a maximum lift coefficient (C_{Lmax}) of 0.89 and 0.91, respectively. However, the C and D UAV configurations (both with amplitude, $a = 0.05c$) delay it up to $\alpha = 20°$ with reference to the baseline wing with a maximum lift coefficient of 0.90 and 0.93, respectively. There is no significant difference in the lift coefficient between A and B-configurations, nor between C and D configurations. The incorporation of tubercles on the leading edge of the wing generates swirling vortices that energize the boundary layer and delay flow separation. Consequently, these data demonstrate improved control at higher angles of attack. Due to the delayed stall, these modified UAV wings can achieve higher lift coefficients at greater angles of attack compared to the baseline case.

It can be concluded that a higher amplitude produces a greater stall delay, regardless of wavelength. However, a shorter wavelength ($\lambda = 0.25c$) generates a higher lift coefficient in the configurations with the same amplitude. Consequently, the B-configuration ($a = 0.03c$; $\lambda = 0.25c$) presents the highest lift value at $\alpha = 15°$ compared to A-UAV ($a = 0.03c$; $\lambda = 0.5c$), and similarly, the D-configuration ($a = 0.05c$; $\lambda = 0.25c$) presents the highest lift coefficient at $\alpha = 20°$ compared to C-UAV ($a = 0.05c$; $\lambda = 0.5c$). Among all the modified wing configurations, the C configuration produces the highest lift coefficient and the greatest delay in stall.

Fig. 5 shows the drag coefficient (C_D) for the baseline case and the four modified wing configurations. For positive angles of attack, the baseline case (red curve) presents the lowest drag coefficient values. These results were expected because the incorporation of tubercles on the leading edge of the wing increases surface roughness and disrupt airflow, leading for greater drag. The tubercles, while potentially beneficial for enhancing lift coefficient and delaying stall (as explained above), inherently generate additional aerodynamic drag, resulting in higher drag coefficients compared to the baseline case (smooth leading edge).

The modified configurations exhibit similar drag coefficients at all angles of attack except for negative angles of attack. Under this condition, B and D-UAV configurations (both with wavelength, $\lambda = 0.25c$) present the lowest drag coefficient values, regardless of amplitude.

Fig. 6 presents the aerodynamic efficiency (E) for the baseline case and the four UAV configurations. From $\alpha = 0°$ to $\alpha = 15°$, the baseline case exhibits the highest aerodynamic efficiency compared to the other configurations. At $\alpha \geq 15°$, all configurations, including the baseline case, show similar values of aerodynamic efficiency. In the modified UAV configurations, the aerodynamic efficiency is negatively impacted. While the lift coefficient (C_L) benefits are significant at higher angles of attack, the increase in aerodynamic drag outweighs these benefits at lower angles of attack, leading to reduced overall aerodynamic efficiency.

Fig. 7 presents the percentage variation of the lift coefficient for the four modified UAV configurations compared to the baseline case. At $\alpha = 10°$, when the baseline case reaches the stall condition, only the A-UAV configuration shows a higher lift coefficient, approximately 2.5 % higher. However, the other modified configurations have a lower lift coefficient than the baseline case at this angle of attack.

At $\alpha = 15°$, the stall condition occurs for the A and B configurations (both with amplitude, $a = 0.03c$), with lift coefficients up to 12.5 % and

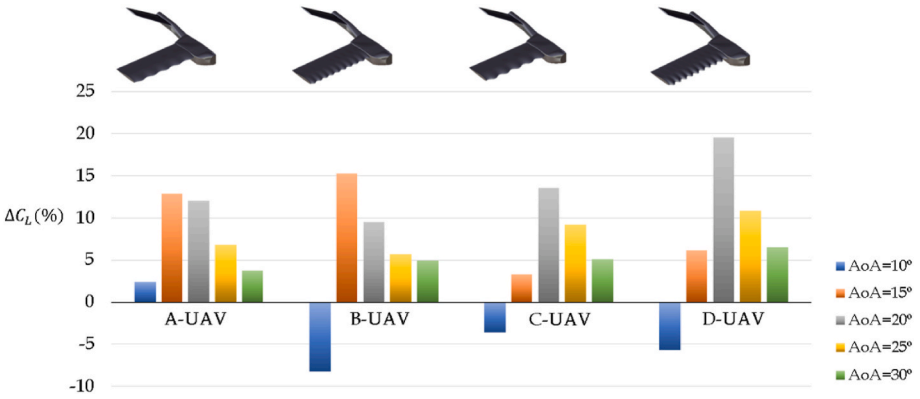


Fig. 7. Percentage variation in lift coefficient for higher angles of attack.

15 % higher than the baseline case, respectively. In this condition, the other two modified configurations, C and D UAV (both with amplitude, $a = 0.05c$) exhibit lift coefficients up to 4 % and 6 % higher than the baseline case, respectively.

Complete flow separation occurs at $\alpha = 20^{\circ}$ for the C and D configurations, with lift coefficients up to 14 % and 20 % higher than the baseline case, respectively. For higher angles of attack, C- and D-configurations presents higher lift coefficients, with the D configuration (amplitude, $a = 0.05c$ and wavelength $\lambda = 0.25c$) exhibiting a slightly higher lift coefficient.

Fig. 8 shows the streamlines for the baseline case and for the modified wing with tubercles (D-configuration) for various angles of attack (α). To obtain a more detailed visualization of the flow, only the half-model and the most representative angles of attack have been shown.

The streamlines show the formation of the wingtip vortex, which starts at the leading edge of the wing. The flow spirals in a clockwise direction. As the angle of attack increases, the velocity of the flow at the origin of the vortex increases (red zone) with velocities up to 10 % above the freestream velocity. Additionally, this wingtip vortex increases in size with the angle of attack.

In the baseline case, a series of blue streamlines with low velocities, close to zero, reveal a separation of the flow over the wing at an angle of attack of 10°, indicating that the vehicle is entering the stall region. However, in the modified wing configuration with tubercles, a series of swirling vortices begin to form over the wing due to the sinusoidal leading-edge configuration, which allows for flow adhesion at higher

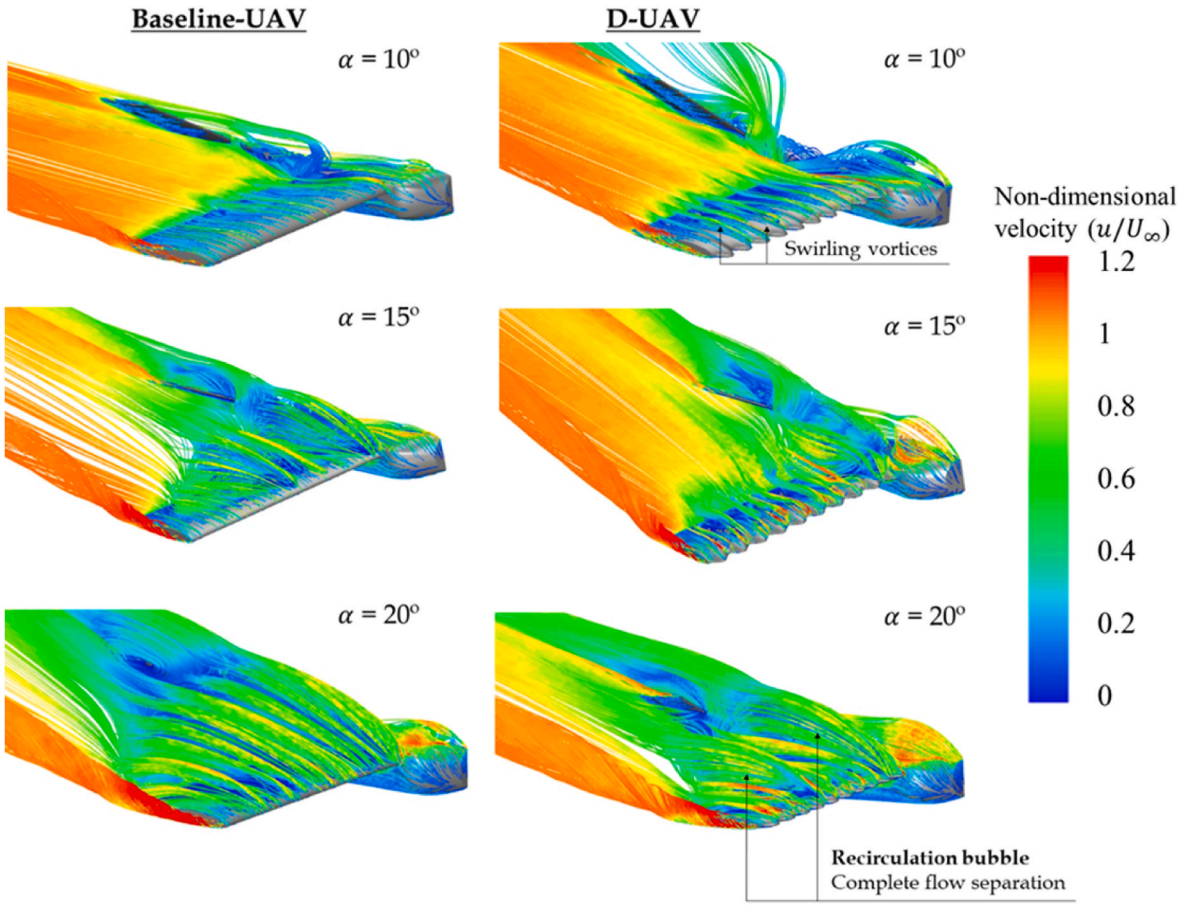


Fig. 8. Streamlines of non-dimensional velocity for the baseline case and the D-UAV configuration.

angles of attack. This phenomenon is observed more clearly at an angle of attack of 15°. In this case, the tubercle configuration shows the formation of small swirling vortices that keep the flow attached, whereas in the baseline configuration, the flow is separated, forming a notable recirculation bubble (blue streamlines).

At an angle of attack of 20°, it is observed that the flow is separated in both configurations. In the baseline case, the recirculation bubble is larger, approximately twice the size of that in the modified wing configuration with tubercles.

5. Conclusions

The influence of leading-edge tubercles on the aerodynamic characteristics of a typical UAV with a rectangular wing composed of Eppler 1876 airfoils was investigated using CFD simulations at a Reynolds number of $1.3 \bullet 10^5$. The wing was modified to include tubercles at the leading-edge, and four modified wing configurations with constant wavelength and amplitude along the span were analyzed.

All modified wing configurations improved lift characteristics in the post-stall region compared to the baseline case, resulting in higher stall angles and maximum lift coefficients (C_{Lmax}). The A- and B-configurations (with amplitude $a = 0.03c$) delayed stall to an angle of attack of 15°, while the C- and D-configurations delayed it to 20 ° compared to the baseline case. The results demonstrated that the D configuration (amplitude $a = 0.05c$ and wavelength $\lambda = 0.25c$) achieved the highest C_{Lmax} of up to 17 % compared to the baseline case while maintaining the greatest stall delay.

Flow visualization at most interesting angles of attack was also presented. At $\alpha = 10^o$, the flow was detached from the wing in the baseline case, while it remained attached in the wing configuration with tubercles, with swirling vortices forming. At $\alpha = 20^o$, the modified wing and the baseline case exhibited completely flow detachment.

The tubercles, inspired by the flippers of humpback whales, create a series of swirling vortices along the wing's leading edge, enhancing airflow attachment and delaying flow separation. This study goes beyond merely identifying these benefits by also investigating the effects of different wavelengths and amplitudes of the tubercles. By analyzing various tubercle configurations, the research provides a comprehensive understanding of how these parameters influence aerodynamic performance.

The findings offer valuable insights into optimizing UAV designs for improved performance, especially in applications requiring high maneuverability and stability under variable conditions. Specifically, these results study demonstrates that incorporating tubercles on the leading edge of a typical UAV wing composed of Eppler 186 significantly improves lift characteristics in the post-stall region.

CRediT authorship contribution statement

Rafael Bardera: Writing – review & editing, Validation, Supervision, Resources, Methodology, Investigation, Formal analysis, Conceptualization. **Ángel Antonio Rodríguez-Sevillano:** Writing – review & editing, Supervision, Methodology, Formal analysis, Conceptualization. **Estela Barroso-Barderas:** Writing – review & editing, Visualization, Validation, Software, Methodology, Investigation, Data curation. **Juan Carlos Matías-García:** Writing – review & editing, Writing – original draft, Visualization, Validation, Software, Methodology, Investigation, Data curation, Conceptualization.

Declaration of competing interest

The authors declare that they have no known competing financial interests or personal relationships that could have appeared to influence the work reported in this paper.

Data availability

No data was used for the research described in the article.

Acknowledgments

The authors would like to thank the staff of the Experimental Aerodynamics department of INTA who participated in the tests presented in this paper. This study is included in the "Termofluidodinámica" program 464A 64 1999 14 205 0005 of the Spanish Ministry of Defense with INTA internal code IDATEC S.IGB21001. Thanks also to the collaboration between the Experimental Aerodynamics department of INTA and Technical University of Madrid (UPM).

References

[1] R. Austin, Unmanned Aircraft Systems: UAVS Design, Development and Deployment, vol. 54, John Wiley & Sons, 2011.
[2] P. Marques, Emerging technologies in UAV aerodynamics, International Journal of Unmanned Systems Engineering 1 (2013) 3–4, https://doi.org/10.14323/ijuseng.2013.2.
[3] J. Flake, B. Frischknecht, S. Hansen, N. Knoebel, J. Ostler, B. Tuley, Development of the stableyes unmanned Air vehicle. 8th International Micro Air Vehicle Competition, The University of Arizona, Tucson, AZ, 2004, pp. 1–10.
[4] J. Han, Z. Hui, F. Tian, G. Chen, Review on bio-inspired flight systems and bionic aerodynamics, Chin. J. Aeronaut. 34 (7) (2021) 170–186.
[5] K.L. Hansen, R.M. Kelso, B.B. Dally, Performance variations of leading-edge tubercles for distinct airfoil profiles, AIAA J. 49 (1) (2011) 185–194.
[6] G. Moscato, J. Mohamed, Improving performances of biomimetic wings with leading edge tubercles'', Exp. Fluid 63 (2022) 146, https://doi.org/10.1007/s00348-022-03493-8.
[7] D.S. Miklosovic, M.M. Murray, L.E. Howle, F.E. Fish, Leading-edge tubercles delay stall on humpback whale flippers, Phys. Fluids 16 (5) (2004) 39–42.
[8] Z. Wei, T.H. New, Y.D. Cui, 'Aerodynamic performance and surface flow structures of leading edge tubercled tapered swept back wings, AIAA J. 56 (1) (2017) 423–431, https://doi.org/10.2514/1.J055663.
[9] M. Seyhan, H. Akbiyik, M. Sarioglu, Kececioglu S. Ceren, ''The effect of leading-edge tubercle on a tapered swept-back SD7032 airfoil at a low Reynolds number'', Ocean Engineering 266 (2022) https://doi.org/10.1016/j.oceaneng.2022.112794.
[10] M.M. Murray, F.E. Fish, L.E. Howle, D.S. Miklosovic, Effects of leading-edge tubercles on a representative whale flipper model at various sweep angles, in: Proceedings of the Fourteenth International Symposium on Unmanned Untethered Submersible Technology (UUST), NH, Autonomous Undersea Systems Inst., Lee, 2005.
[11] E. Sudhakar, N. Karthikeyan, 'Effect of Leading Edge Tubercles on Flow Field over NACA-4415 Airfoil at Low Reynolds Number'', The 14th Asian Congress of Fluid Mechanics, 2013.
[12] S. Sudhakar, N. Karthikeyan, L. Venkatakrishnan, ''Influence of Leading Edge tubercles on aerodynamic characteristics of a high aspect-ratio UAV'', Aero. Sci. Technol. 69 (2017) 281–289, https://doi.org/10.1016/j.ast.2017.06.031.
[13] H. Johari, C. Henoch, D. Custodio, A. Levshin, Effect of leading-edge protuberances on aerofoil performance, AIAA J. 45 (11) (2007) 2634–2642.
[14] J. Li, C. Liu, X. Li, 'Effects of wavy leading-edge protuberance on hydrofoil performance and its flow mechanism, J. Mar. Sci. Eng. 9 (2021) 1138, https://doi.org/10.3390/jmse9101138. MDPI.
[15] Z. Ni, Tsung-chow Su and Manhar Dhanak, ''An empirically-based model for the lift coefficients of twisted airfoils with leading-edge tubercles'', IP Advancs 8 (2018) 045123 https://doi.org/10.1063/1.5023103.
[16] E. Barroso-Barderas, Á.A. Rodríguez-Sevillano, R. Bardera-Mora, J. Crespo-Moreno, J.C. Matías-García, Design of non-Conventional flight control systems for bioinspired micro Air vehicles, Drones 6 (9) (2022) 248.